Key Engineering Materials
ISSN: 1662-9795, Vol. 926, pp 242-249
doi:10.4028/p-zg7019

Submitted: 2022-02-03
Revised: 2022-02-24
Accepted: 2022-02-25
Online: 2022-07-22

Laser Powder Bed Fusion of Aluminium Alloy 6061 for Ultra-High Vacuum Applications

Ronan McCann[1,2,3,4,a*], Cian Hughes[1,2,b], Dermot Brabazon[1,2,3,4,c]

[1]I-Form Advanced Manufacturing Research Centre, Ireland

[2]Advanced Processing Technology Research Centre, School of Mechanical and Manufacturing Engineering, Dublin City University, Glasnevin, Dublin 9, Ireland

[3]National Centre for Sensor Research (NCSR), Dublin City University, Glasnevin, Dublin 9, Ireland

[4]National Centre for Plasma Science and Technology (NCPST), Dublin City University, Glasnevin, Dublin 9, Ireland

[a]ronan.mccann@i-form.ie, cian. [b]hughes@dcu.ie, [c]dermot.brabazon@dcu.ie

Keywords: additive manufacturing, laser powder bed fusion, aluminium, 6061,

Abstract. As additive techniques such as laser powder bed fusion find increasing adoption industry, the ability to adapt these processes to industrially relevant materials is paramount. This adaptation can represent a significant challenge when working with wrought alloy feedstocks, which often result in brittle or porous parts lacking the mechanical properties of their conventionally wrought counterparts. One such alloy, aluminium 6061, is a highly used alloy in the aerospace, automotive, and semiconductor manufacturing industries. The conventionally manufactured components can have complex morphologies and may be assemblies of multiple individual components. As such, the ability to use an additive approach, and produce these as single parts can lead to significant benefits.

In this work, we examine laser powder bed fusion of aluminium alloy 6061. The effects of process parameters such as laser power, beam scan speed, hatching distance, spot size was examined with a view towards developing an optimised process for this traditionally wrought alloy. Parts were examined for porosity and microstructure, with an aim to develop greater than 95% relative densities. To aid in process optimisation, in-situ pyrometry was deployed to understand the effects of the process parameters and develop a robust and repeatable process for producing 6061 components.

Introduction

Over the previous decade, Additive Manufacturing (AM) has gained acceptance in production environments and as such there is a growing need to adapt materials currently used in conventional manufacturing techniques to AM processes. While commonly used materials such as stainless steels have been very easily adapted to AM processes [1,2]. The AM approach allows for unique geometries which can simplify the fabrication and assembly of complex parts which leads to savings in both time and cost in production environments.

For complex additive techniques such as Laser Powder Bed Fusion (L-PBF), the ability to adapt to industrially relevant materials is paramount. This adaptation can represent a significant challenge when working with wrought alloy feedstocks, which often result in brittle or porous parts lacking the mechanical properties of their conventionally wrought counterparts [3]. One such alloy, aluminium 6061, is a highly used alloy in the aerospace, automotive, and plasma manufacturing tool industries [1,4]. The conventionally manufactured components can have complex morphologies and may be assemblies of multiple individual components [5]. As such, the ability to use an additive approach, and produce these as single parts can lead to significant benefits.

In this paper we present the production of aluminium components via L-PBF. Part properties such as microstructure, porosity and density, or examined with a view to develop high density, low porosity components suitable for ultra-high vacuum applications. Also examined was the use of in-situ process monitoring via IR pyrometry with a view to develop a robust process for aluminium alloy 6061.

Materials and Methods

In this study, samples were produced on an Aconity Mini (Aconity3D Gmbh, Germany) which had a maximum build volume of 140 mm diameter x 200 mm height and used an aluminium alloy 6082-T6 build plate. The system was fitted with a fibre laser with a maximum power output of 200 W operating in continuous wave mode. To examine the capability of the system to manufacture high density aluminium 6061 parts without the requirement of powder bed preheating, the tests were conducted with the powder bed at ambient temperature. The samples produced were 10 mm x 10 mm x 15 mm cuboids and were printed without supporting structures to ensure good adhesion of the first layer to the build plate. For all the produced samples, a layer height of 60 µm was used and the scanning direction was rotated by 90° after each layer. The feedstock material used for this study was gas atomized aluminium alloy 6061 (20-63 µm) sourced from Carpenter Additive, the composition of which is shown in Table 1. Prior to commencing the process, the build chamber was purged with ultrapure argon (>99.999%) until an oxygen concentration of <20 ppm was achieved.

For in-situ process monitoring, the Aconity Mini system was fitted with a pyrometer in-line with the laser beam allowing imaging of the meltpool and allowing investigation into the thermal behaviour of the meltpool.

Table 1: Composition of the Al6061 powder used in this study.

Element	Min (wt%)	Max (wt%)
Al	Balance	-
Zn	0	0.25
Ti	0	0.15
Si	0.4	0.8
Mn	0	0.15
Mg	0.8	1.2
Fe	0	0.7
Cu	0.15	0.4
Cr	0	0.35
Other	0	0.15

This study employed a design of experiments methodology to develop a process map of the process space. Three Box-Behnken designs were used to map the process space, each with three input factors resulting in 51 datapoints which was analysed using DesignExpert 11 (StatEase Inc. USA). The input factors are listed in Table 2. The three input factors for the experimental design were laser power, beam scan speed and hatching distance. One additional input factor, laser spot size was fixed for each of the three experimental designs. A full quadratic model was developed along with corresponding ANOVA analysis.

Table 2: Input factors used in the Box-Behnken design for this study.

Run	Spot Size (um)	Laser Power (W)	Scan Speed (mm/s)	Hatching Distance (um)	Relative Density (%)
1	60	190	600	150	95.28
2	60	200	1000	120	94.82
3	60	180	800	90	94.62
4	60	200	800	150	94.79
5	60	190	800	120	95.08
6	60	190	800	120	94.42
7	60	180	600	120	94.44
8	60	190	1000	150	94.89
9	60	190	1000	90	94.96
10	60	190	600	90	95.00
11	60	190	800	120	94.87
12	60	180	800	150	94.78
13	60	180	1000	120	95.04
14	60	200	600	120	94.65
15	60	200	800	90	95.04
16	60	190	800	120	95.08
17	60	190	800	120	95.04
18	75	190	600	150	93.87
19	75	200	1000	120	94.59
20	75	180	800	90	94.40
21	75	200	800	150	93.90
22	75	190	800	120	94.43
23	75	190	800	120	94.37
24	75	180	600	120	94.54
25	75	190	1000	150	93.89
26	75	190	1000	90	94.10
27	75	190	600	90	94.41
28	75	190	800	120	93.74
29	75	180	800	150	94.15
30	75	180	1000	120	94.28
31	75	200	600	120	94.26
32	75	200	800	90	93.99
33	75	190	800	120	94.13
34	75	190	800	120	94.13
35	90	190	600	150	95.49
36	90	200	1000	120	95.29
37	90	180	800	90	95.14
38	90	200	800	150	95.27
39	90	190	800	120	95.26
40	90	190	800	120	94.92
41	90	180	600	120	94.87

42	90	190	1000	150	95.40
43	90	190	1000	90	95.13
44	90	190	600	90	94.89
45	90	190	800	120	95.21
46	90	180	800	150	95.19
47	90	180	1000	120	95.00
48	90	200	600	120	94.89
49	90	200	800	90	95.10
50	90	190	800	120	94.91
51	90	190	800	120	95.14

Microstructure analysis was performed using an LS-15 scanning electron microscope (Zeiss, Switzerland). Prior to imaging the samples were polished and etched using Keller's Reagent to reveal the underlying part porosity and microstructure. Density determination was performed using the Archimedes method through comparison of the sample weight in air and in water. For the relative density calculations, a value of 2.70 g/cm^3 was used for 100% density aluminium 6061.

Results and Discussion

In-situ Pyrometry. Figure 1 shows the recorded signal from pyrometer for a single layer at a height of 6.6 mm. Significant variation is seen across the build area which was attributed to the direction of the process gas, with parts nearer the gas inlet exhibiting cooler meltpool IR signals. While all process parameters trialed successfully fabricated parts, the variation in IR signal may be indicative of a larger processed bias present in the arrangement of the parts on the build plate. This result highlights the importance of optimal build orientation when conducting DOE tests which may result in process bias or unexpected results. The variation within individual parts, may be indicative of the potential for lack of fusion defects, contributing to increased porosity [6].

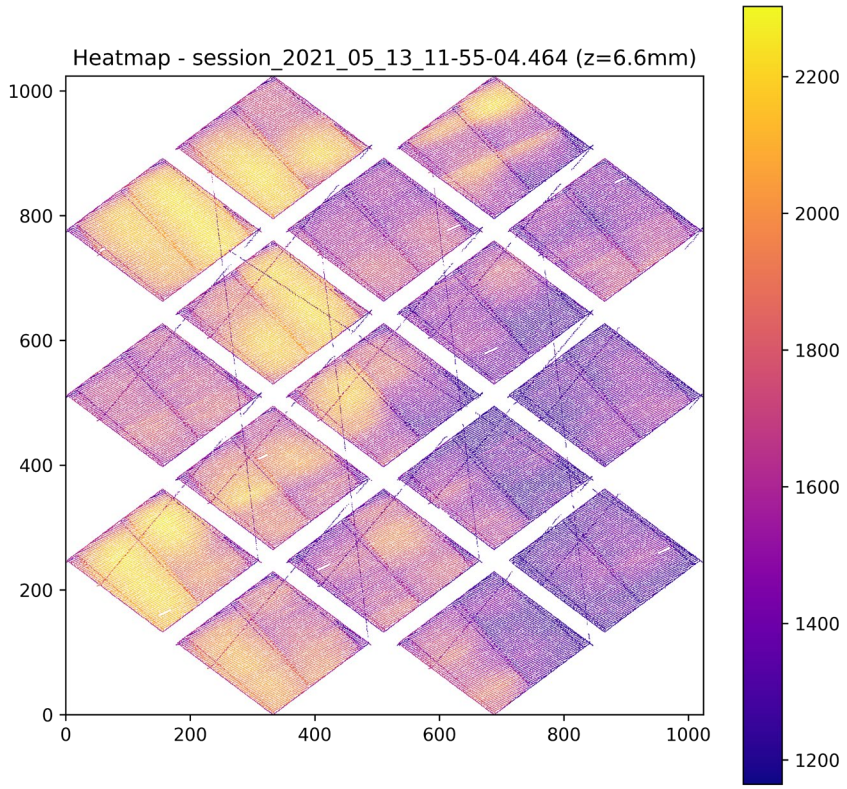

Figure 1: An acquired pyrometry signal at a height of 6.6 mm during the build.

Relative Density. Figure 2 shows the spread of relative densities for the DoE. In general, the relative densities determined were within 2% of the mean density of 94.73% ± 0.48%. This result is indicative that the process space examined was stable, however for higher densities to be achieved, the process space must be widened for further studies. Figure 3 shows the quadratic model developed for relative density as determined via the Archemdies method at a laser power of 190 W and a spot size of 150 µm. The average relative density was 94.7 ± 0.46%, with a maximum of 93.7% and a minimum of 75.0%. These results compare favourably to prevous work on 6061 also conducted both with and without the use of preheating of the powder bed [4]. These results suggest that for a wide range of applications, the use of preheating may be omitted, thus simplifying and reducing the time needed to produce parts. It should be noted that the geometries used in this study are simplistic, and these results may be different to those when complex geometries which would have radically different thermal gradients and cooling behavours. The DoE modelling suggested that spot size was the most significant input factor with both higher densities seen at the smallest and largest spot sizes used, both exceeding 95%, while the lowest densities were 93.4%. The model adjusted R-squared was 0.695 which was in agreement of the model predicted R-squared of 0.546.

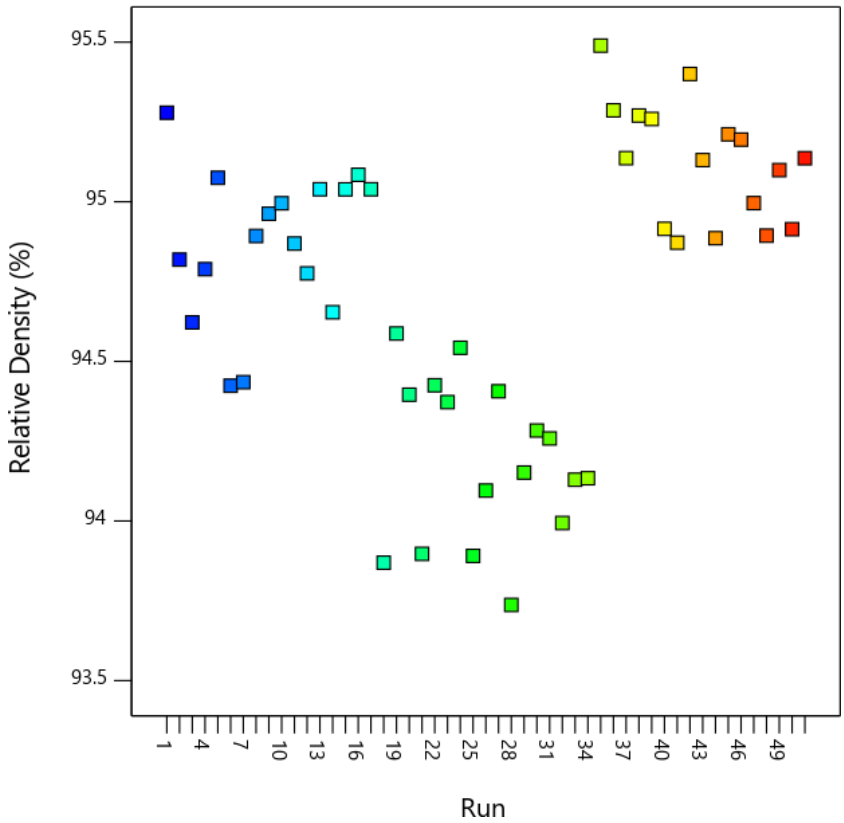

Figure 2: Relative densities of the produced samples fabricated.

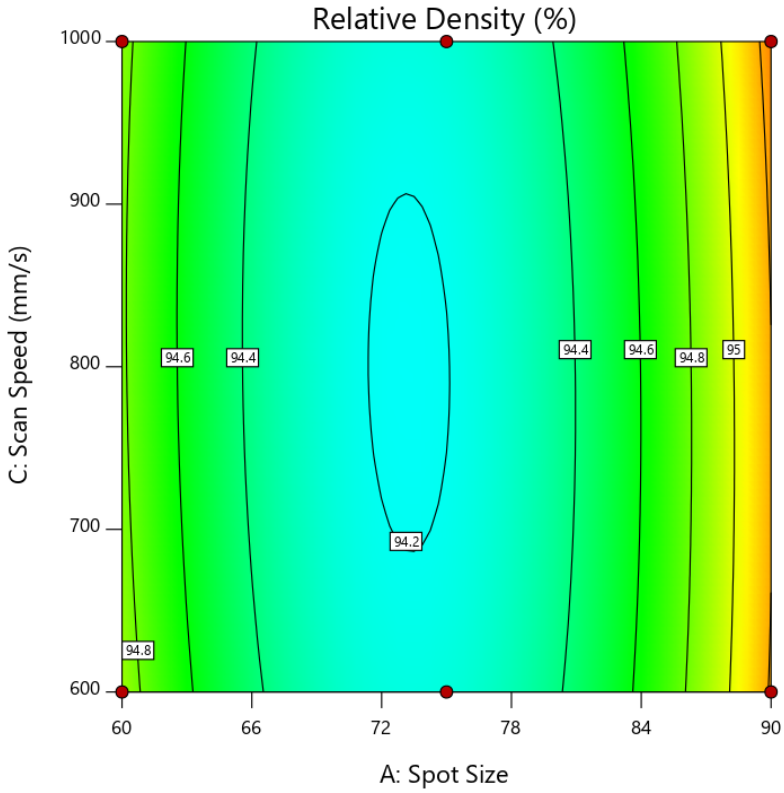

Figure 3: Relative density of the produced samples as determined via the Archimedes method at a and a hatching distance of 150 µm.

Microstructure. Scanning electron microscopy was used to examine the part surface microstructure, an example of which is shown in Figure 4. While the grain structure was not visible, a significant number of cracks were seen in both the cross-sectional (Figure 4a) and longitudinal (Figure 4b) directions of the parts as built. Hot cracking is a significant challenge for aluminium parts in L-PBF, in particular when working with wrought feedstocks such as 6000- and 7000-series aluminium alloys [7]. While previous studies have suggested that pre-heating can partially mitigate hot cracking in aluminium parts fabricated via L-PBF, this presents additional process complexity, and challenges such as reduced build volume in some systems. An alternative mitigation route is the use of grain refiner, well established in other fabrication technologies such as casting which presents an interesting area of investigation for adapting feedstocks for PBF techniques [8,9].

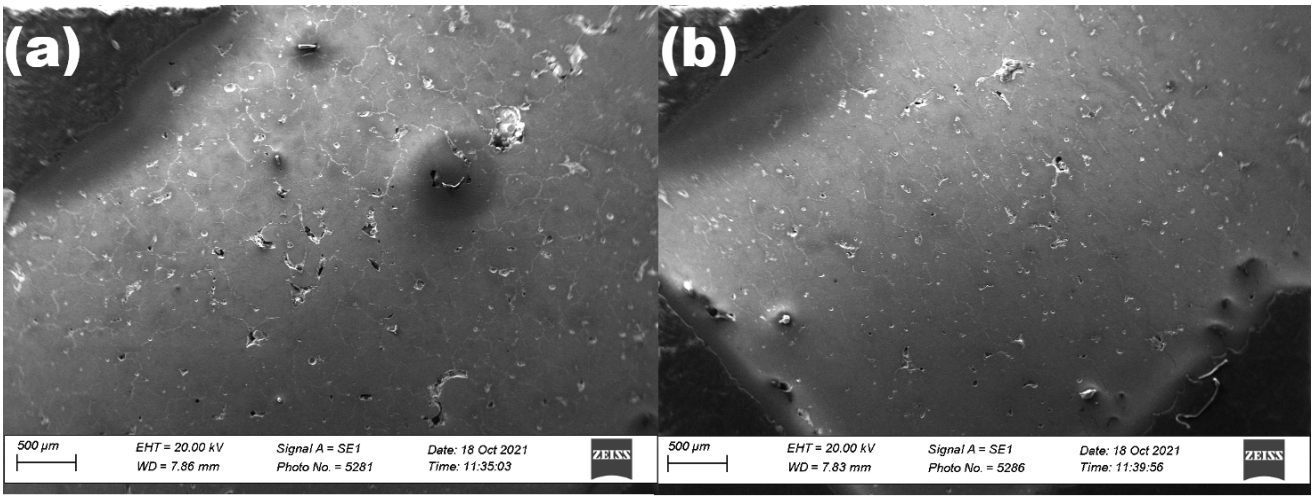

Figure 4: Images recorded via scanning electron microscopy showing the (a) cross-sectional (xy) and (b) transverse (z) orientations.

Conclusions

This work presented an intitial investigation into the fabrication of aluminium 6061 parts using L-PBF and a Box-Behnken design of experiments methodology. In-situ pyrometry was used to visualise the meltpool behaviour during the build, and part density and microstructure examined post-build. The main results were:

- Archemedian density analysis revealed maximum part densities of 95%, which compared favourably with those in the literature.
- Electron microscopy showed significant hot cracking in both the transverse and cross-sectional directions, which may lower the mechanical properties of the parts compared to conventionally producted parts.
- In-situ pyrometry revealed variation in the meltpool temperature as a function of part position, highlighting the effect of process gas cooling on the parts, which could result in error when developing a process space map. However, the produced model was seen to have a high adjusted R-squared value of 0.6945 which was in agreement with the model predicted R-squared.

Future work will include the confimration of the produced model using optimial process parameters, and an examination of the use of grain refiners which may allow a reduction in the hot cracking behaviour seen [8]. Futher work on the analysis of the part microstructure using techniques such as Electron Backscatter Diffraction (EBSD) will allow further illucidation of the cooling mechanisms present during the build, which may reveal furter information to allow part densities above those seen in this study [7].

Acknowledgements

This publication has emanated from research supported by the European Union's Horizon 2020 Research and Innovation Program under grant agreement No. 862100, the Irish Research Council under Grant Number NF/2019/15931397, and Science Foundation Ireland (SFI) under Grant Number 16/RC/3872 and is co-funded under the European Regional Development Fund and by I-Form industry partners.

References

[1] J.H. Martin, B.D. Yahata, J.M. Hundley, J.A. Mayer, T.A. Schaedler, T.M. Pollock, 3D printing of high-strength aluminium alloys, Nature. 549 (2017) 365–369.

[2] P.J. DePond, G. Guss, S. Ly, N.P. Calta, D. Deane, S. Khairallah, M.J. Matthews, In situ measurements of layer roughness during laser powder bed fusion additive manufacturing using low coherence scanning interferometry, Mater. Des. 154 (2018) 347–359.

[3] H.E. Sabzi, S. Maeng, X. Liang, M. Simonelli, N.T. Aboulkhair, P.E.J. Rivera-Díaz-del-Castillo, Controlling crack formation and porosity in laser powder bed fusion: Alloy design and process optimisation, Addit. Manuf. 34 (2020) 101360.

[4] S.Z. Uddin, L.E. Murr, C.A. Terrazas, P. Morton, D.A. Roberson, R.B. Wicker, Processing and characterization of crack-free aluminum 6061 using high-temperature heating in laser powder bed fusion additive manufacturing, Addit. Manuf. 22 (2018) 405–415.

[5] W. Gao, Y. Zhang, D. Ramanujan, K. Ramani, Y. Chen, C.B. Williams, C.C.L. Wang, Y.C. Shin, S. Zhang, P.D. Zavattieri, The status, challenges, and future of additive manufacturing in engineering, CAD Comput. Aided Des. 69 (2015) 65–89.

[6] G. Mohr, S.J. Altenburg, A. Ulbricht, P. Heinrich, D. Baum, C. Maierhofer, K. Hilgenberg, In-Situ Defect Detection in Laser Powder Bed Fusion by Using Thermography and Optical Tomography—Comparison to Computed Tomography, Metals (Basel). 10 (2020) 103.

[7] N.T. Aboulkhair, M. Simonelli, L. Parry, I. Ashcroft, C. Tuck, R. Hague, 3D printing of Aluminium alloys: Additive Manufacturing of Aluminium alloys using selective laser melting, Prog. Mater. Sci. 106 (2019) 100578.

[8] D. Zhang, A. Prasad, M.J. Bermingham, C.J. Todaro, M.J. Benoit, M.N. Patel, D. Qiu, D.H. StJohn, M. Qian, M.A. Easton, Grain Refinement of Alloys in Fusion-Based Additive Manufacturing Processes, Metall. Mater. Trans. A Phys. Metall. Mater. Sci. 51 (2020) 4341–4359.

[9] Z. Wang, X. Wang, X. Chen, C. Qiu, Complete columnar-to-equiaxed transition and significant grain refinement in an aluminium alloy by adding Nb particles through laser powder bed fusion, Addit. Manuf. 51 (2022) 102615.